Supplementary Information

Boosting electrocatalytic nitrate reduction to ammonia with a Cu/Ag-Ru tandem catalyst at industrial-scale current density

Ru Jia [a,b,†], Xiaoxue Zhang [a,b,†], Li Gan [a,b], Muhammad Tahir [c], Zhen-Feng Huang [a,b,], Lun Pan [a,b], Ruijie Gao [a,b], Chengxiang Shi [a,b], Xiangwen Zhang [a,b], Guidong Yang [d] and Ji-Jun Zou [a,b,*].*

[a]Key Laboratory for Green Chemical Technology of the Ministry of Education, School of Chemical Engineering and Technology, Institute of Molecular Plus, Tianjin University, Tianjin 300072, China.

[b]Collaborative Innovative Center of Chemical Science and Engineering (Tianjin), Tianjin 300072, China.

[c]Department of Physics, Division of Science and Technology, University of Education, Lahore, 54770, Pakistan.

[d]XJTU-Oxford International Joint Laboratory for Catalysis, School of Chemical Engineering and Technology, Xi'an Jiaotong University, Xi'an, Shaanxi 710049, China.

[*]Corresponding author E-mail address: jj_zou@tju.edu.cn (J.-J. Zou) & zfhuang@tju.edu.cn (Z.-F. Huang).

[†]These authors contributed equally to this work.

S1. Experiment section

1.1. NH_4^+ Quantification

The concentration of produced NH_3 was determined by the indophenol blue method[1]. First, the post-reaction electrolyte was diluted to some extent within the detection range of standard curves. Then, 2 mL of diluted sample was mixed with 2 mL of 1 M NaOH aqueous solution containing 5 wt% sodium citrate and 5 wt% salicylic acid. Next,1 mL of 0.05 M NaClO and 0.2 mL of 1 wt% sodium nitroferricyanide were introduced and the solution was mixed entirely. After standing for 2 h to complete the colour reaction, the absorption spectrum was then measured using an ultraviolet-visible spectrophotometer (UV-2600) in the wavelength range from 550 nm to 750 nm, recording the absorption intensity at a wavelength of 655 nm. A series of different concentrations of NH_4Cl solutions were measured to make calibration curves on the purpose of quantify ammonia.

1.2. NO_2^- Quantification

The post-reaction electrolyte was diluted to some extent within the detection range of standard curves. 5 mL of diluted solution was mixed with 0.1 mL of 1M HCl aqueous solution consisting of 0.5 g sulfonamide. After standing for 10 min, another 0.1 mL solution prepared by 20 mL ultra-pure water and 0.02 g N-(1-naphthyl) ethylenediamine dihydrochloride were introduced[5]. Then the mixture was shaken well and placed in dark for 20 min. The absorption spectrum was measured using an ultraviolet-visible spectrophotometer (UV-2600) in the wavelength range of 450-650 nm, recording the absorption intensity at 540 nm. A series of different concentrations of KNO_2 solutions were measured to make calibration curves on the purpose of quantify nitrite.

1.3. NO_3^- Quantification

Dilute the post-electrolysis electrolyte to an appropriate concentration. Then take out 5 mL of the diluted sample, add 0.10 mL of 2.0 M HCl solution, shake and mix them entirely, and stand for 5 minutes. The absorption spectrum was then measured using an ultraviolet-visible spectrophotometer (UV-2600) in the wavelength range of 200 to 300 nm, recording the absorption intensities at 220 and 275 nm. The final absorbance was calculated by the formula $A = A_{220\ nm} - 2A_{275\ nm}$. A series of standard KNO_3 solutions were used to make a standard concentration-absorbance calibration curve to quantify nitrate.

1.4. Electrochemical active surface area (ECSA) determination

The ECSA is calculated as follows:

$$ECSA = C_{dl}/C_s$$

where C_{dl} is the double layer capacitance and C_s is the specific capacitance of the sample. A general specific capacitance of $C_s = 0.040$ mF cm^{-2} was used in this study and C_{dl} is the slop of half the current difference between anode and cathode versus scan rate at a certain potential. The C_{dl} determination was measured in a potential window from -0.06 V to 0.04 V vs. RHE at different scan rates of 10, 20, 40, 60, 80, 100 mV s^{-1}.

1.5. Reaction order calculation

The calculation of reaction order is based on the formula as follows[2]:

$$NO_3^- + 2H_2O \rightarrow NH_3 + OH^- \quad c = k[NO_3^-]^{\alpha}[H_2O]^{\beta}$$

where, c is the reaction rate of nitrate, k is the reaction rate constant, α, β is the reaction order for nitrate and water, respectively. $[H_2O]^{\beta}$ can be seemed as a constant, due to $[H_2O] \gg [NO_3^-]$. Since the current density j is linear dependent to the reaction rate c ($j = nFc$), the above equation can be rewritten as:

$$ln\, j = K + \alpha\, ln\, [NO_3^-]$$

The reaction order α can be obtained by linearly fit ln j with ln [NO_3^-].

1.6. Electron transfer number calculation

The electron transfer number is calculated according to the Koutecky–Levich equation[3]:

$$\frac{1}{i} = \frac{1}{i_k} + \frac{1}{0.62nFAD_0^{2/3}\omega^{1/2}v^{-1/6}C_0}$$

where i is the current (A), i_k refers to the limiting current (A), n is the electron transfer number, F is the Faraday constant (96,485 C mol^{-1}), A is the specific area of the RDE (0.19625 cm^2), D_0 is the diffusion coefficient of the nitrate (1.80×10^{-5} cm^2 s^{-1})[4], ω is the rotation rate (rpm × 2 π/60, s^{-1}), v is the kinematic viscosity (0.0118 cm^2 s^{-1})[5,6], and C_0 is the bulk concentration of NO_3^- (10×10^{-6} mol cm^{-3}). The inverse of current i (A) is proportional to the inverse of the square root of the rotation rate ($\omega^{-1/2}$). The electron transfer number can be calculated through the slope of the fitted plot.

1.7. Reaction rate constant calculation

Reaction rate constant (k) is analyzed through the formula as follows:

$$C = C_0 \times e^{-kt}$$

Where C is related to real-time concentration of NO_3^- or NO_2^-, C_0 is the initial concentration, k refers to reaction rate constant, and t is the reaction time. On purpose of acquire a deeper insight of the NO_3RR mechanism, we calculate k_1 (NO_3^- to NO_2^-) and k_2 (NO_2^- to NH_3), respectively.

1.8. Calculation of FE, partial current density and NH_3 yield rate

The faraday efficiency (FE) is calculated as follows:

$$FE_{NH_3} = \frac{\left(8 \times F \times C_{NH_3} \times V\right)}{j \times A \times t}$$

$$FE_{NO_2^-} = \left(\frac{2 \times F \times C_{NO_2^-} \times V}{j \times A \times t}\right)$$

The yield rate of NH_3 (Y_{NH3}) is calculated as follows:

$$Y_{NH_3} = \frac{\left(C_{NH_3} \times V\right)}{(A \times t)}$$

Where F is the Faraday constant (96,485 mol^{-1}), C_{NH3} is the molar concentration of NH_3 in post-reaction electrolyte, C_{NO2-} is the molar concentration of NO_2^- in post-reaction electrolyte, V is the volume of the cathodic electrolyte, j is the total current density, A is the electrode geometric area, and t is the reaction time.

The partial current density of NH_3 is calculated as follows:

$$j_{NH3} = j \times FE_{NH3}$$

1.9. Electrochemical online DEMS test

A certain amount of 1 M KOH and 0.1 M KNO_3 as electrolyte was added into a customized electrochemical cell. Catalysts coated on breathable film with gold plating layer, Ag/AgCl electrodes, Pt wire were treated as the working electrode, reference electrode and counter electrode, respectively. Then, a constant potential at 0 V vs. RHE was applied for 60 s and the corresponding mass signals can be detected. After the electrochemical test is completed and the signal returns to the baseline, repeat this procedure another three times.

1.10.Electrochemical in situ ATR-FTIR spectroscopy

In situ ATR-FTIR spectroscopy was obtained with the BRUKER TENSOR. The catalyst ink was prepared by dispersing 6 mg of catalysts in 1 mL of isopropanol solution and then ultrasonicating for 30 min. The NO_3RR was performed in a custom-made H-cell, in which the Hg/HgO and Pt wire were used as reference electrodes and counter electrode,

respectively. Working electrode was fabricated by dropping 50 μL catalyst ink onto the surface of a wedge-shaped silicon coated with a gold layer, with a certain amount of 1 M KOH and 0.1 M KNO_3 as electrolyte. The infrared spectra were measured at different potentials after deducting the background at open-circuit voltage.

S2. Figures and Tables

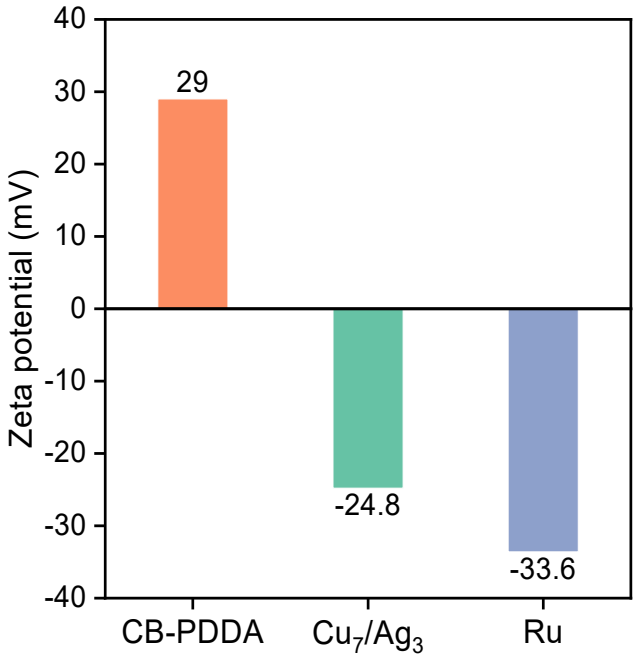

Figure S1. Zeta potentials of CB modified with PDDA, Cu_7/Ag_3 and Ru modified with citrate.

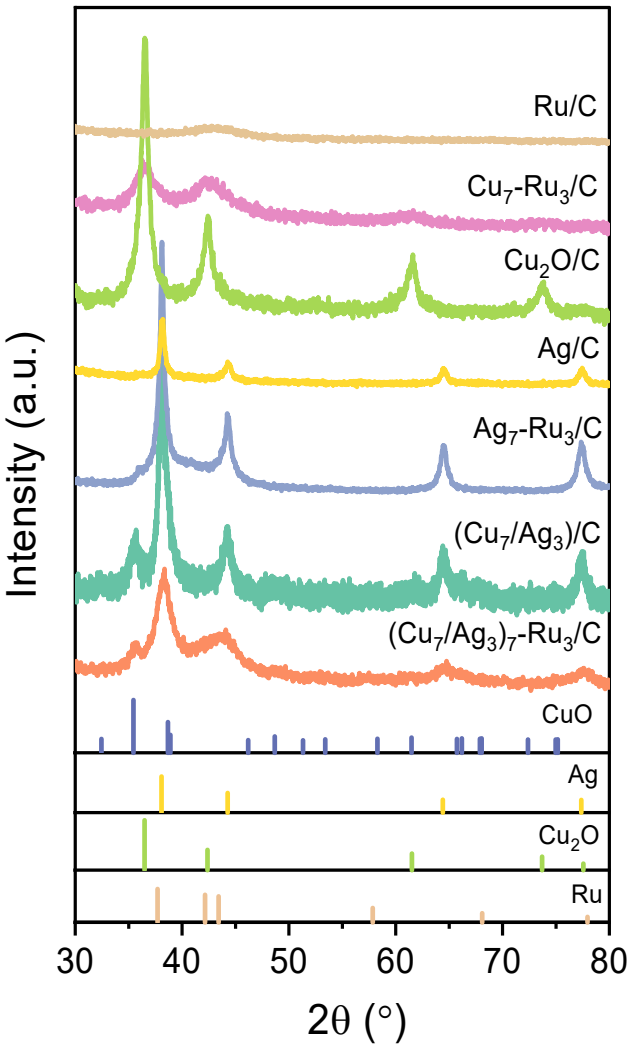

Figure S2. The XRD patterns of Ru/C, Cu_7-Ru_3/C, Cu/C, Ag/C, Ag_7-Ru_3/C, (Cu_7/Ag_3)/C, and (Cu_7/Ag_3)$_7$-Ru_3/C.

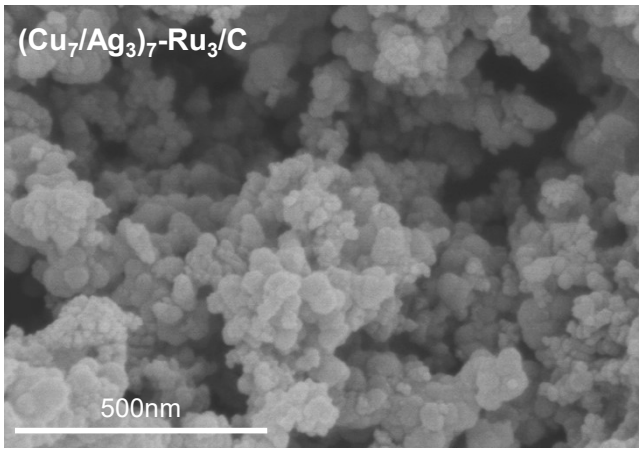

Figure S3. SEM image of $(Cu_7/Ag_3)_7$-Ru_3/C.

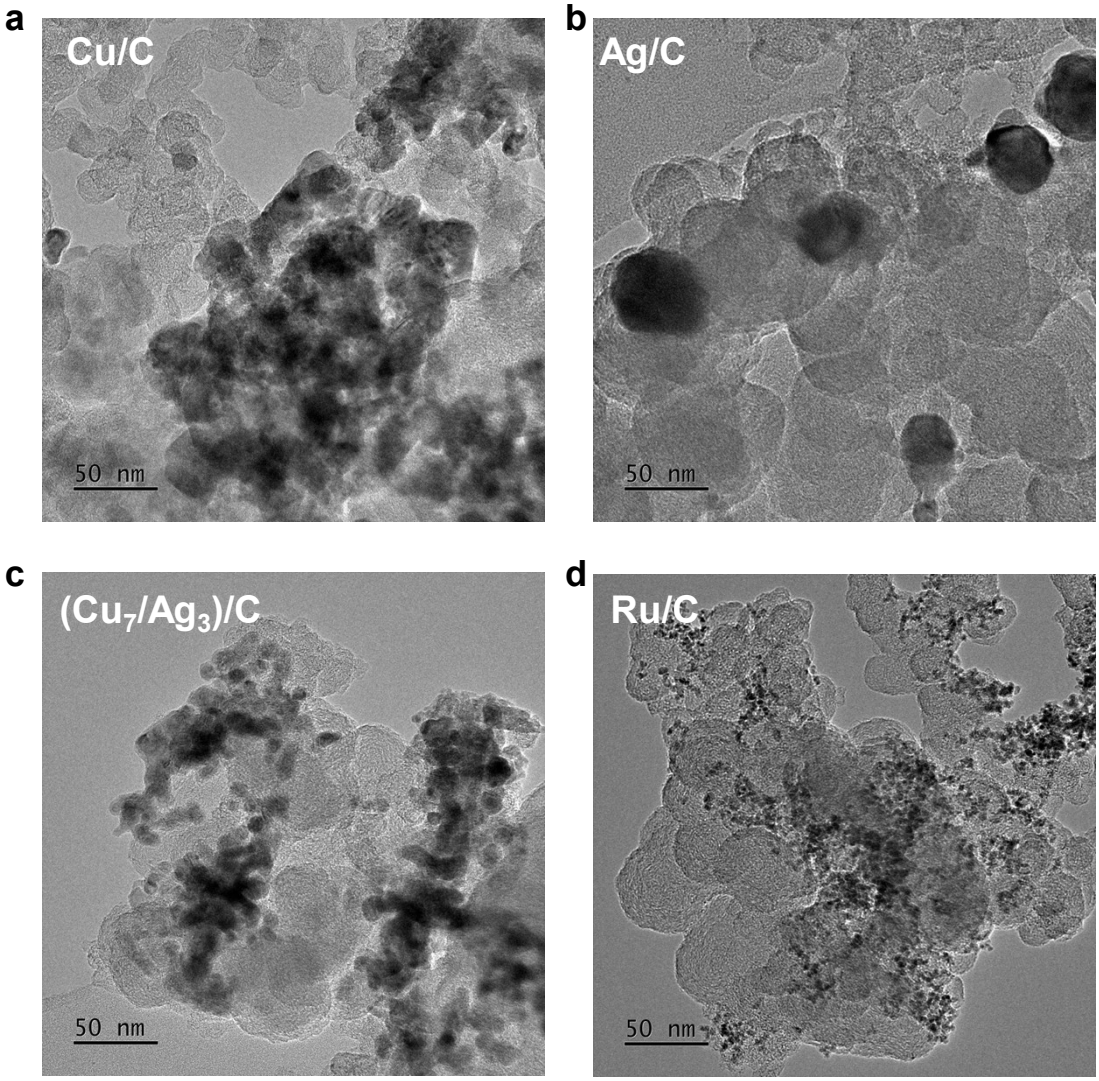

Figure S4. TEM images of Cu/C, Ag/C, Ru/C and $(Cu_7/Ag_3)/C$.

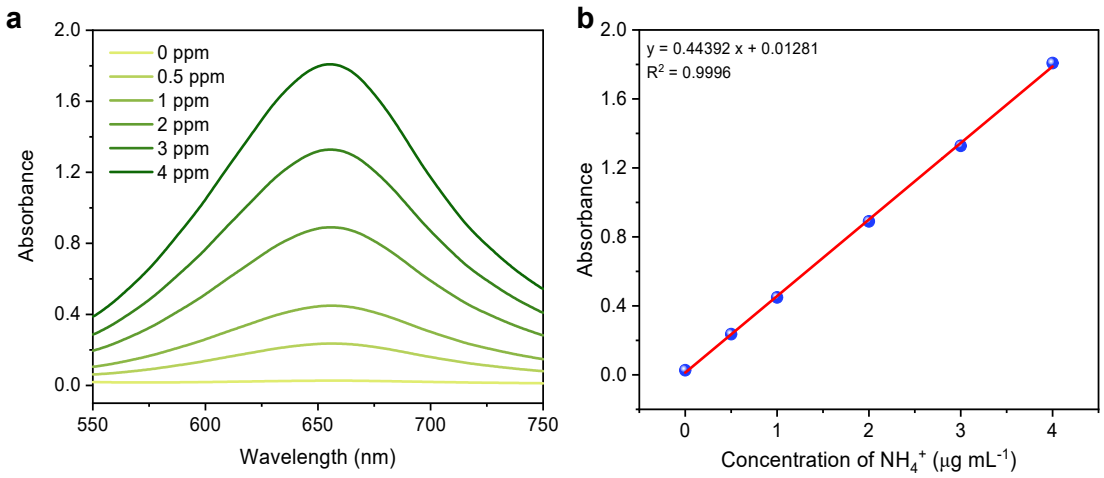

Figure S5. The concentration-absorbance UV-vis calibration curve of NH_3 using different concentration of NH_4Cl solutions as standards. (a) UV-vis curves of indophenol assays with NH_4^+ ions and (b) linear fitting results of the calibration curve.

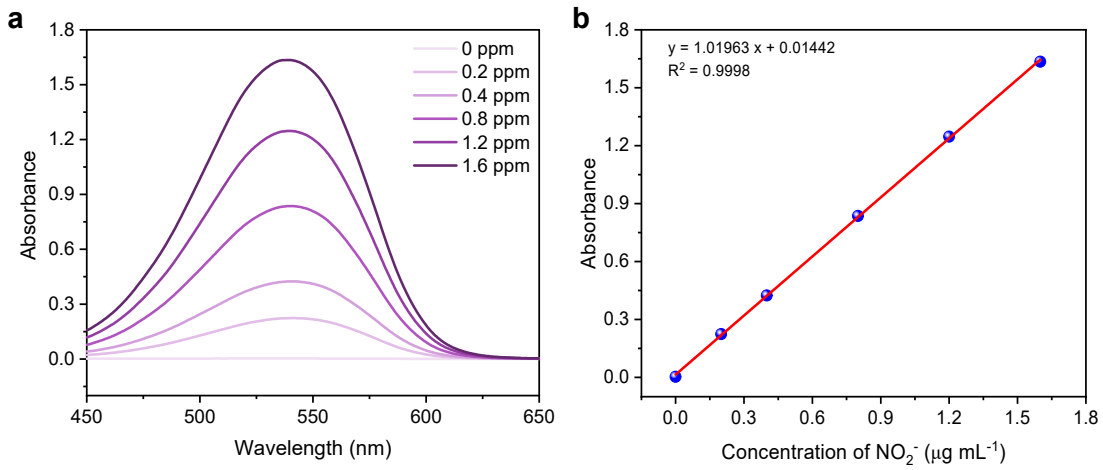

Figure S6. The concentration-absorbance UV-vis calibration curve of NO_2^- using different concentration of KNO_2 solutions as standards. (a) UV-vis curves of assays with NO_2^- ions and (b) linear fitting results of the calibration curve.

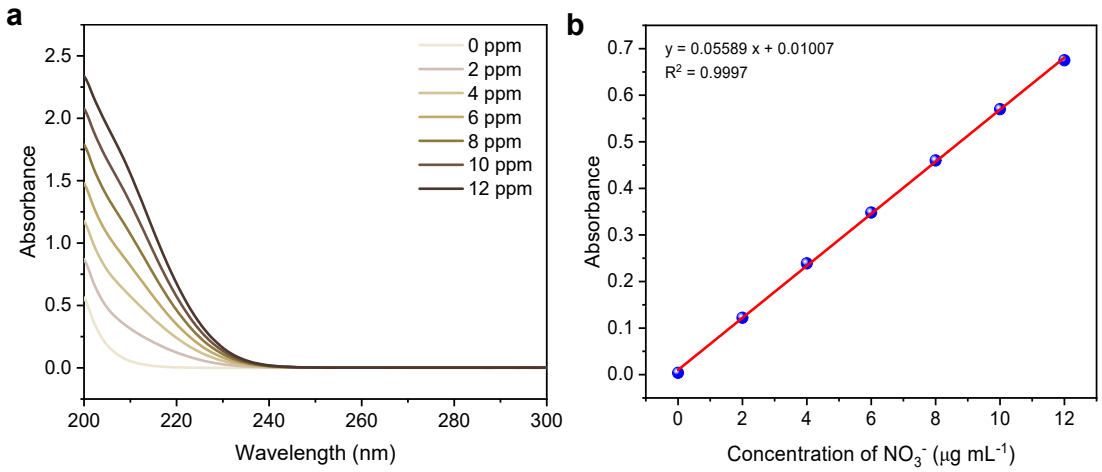

Figure S7. The concentration-absorbance UV-vis calibration curve of NO_3^- using different concentration of KNO_3 solutions as standards. (a) UV-vis curves of assays with NO_3^- ions and (b) linear fitting results of the calibration curve.

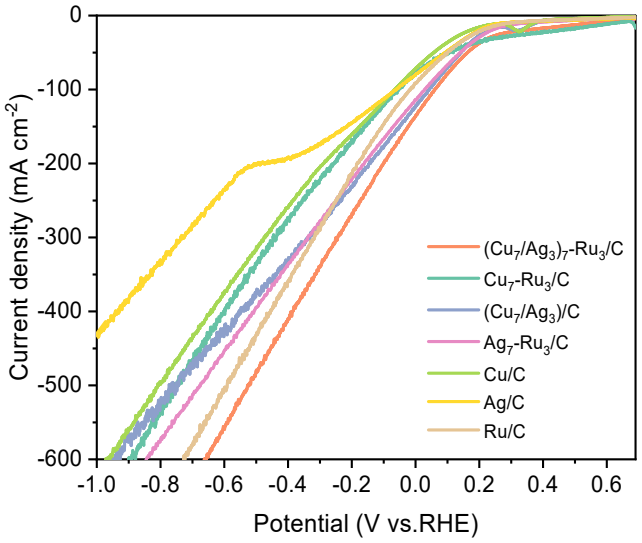

Figure S8. LSV curves of $(Cu_7/Ag_3)_7$-Ru_3/C, Cu_7-Ru_3/C, (Cu_7/Ag_3)/C, Ag_7-Ru_3/C, Cu/C, Ag/C and Ru/C.

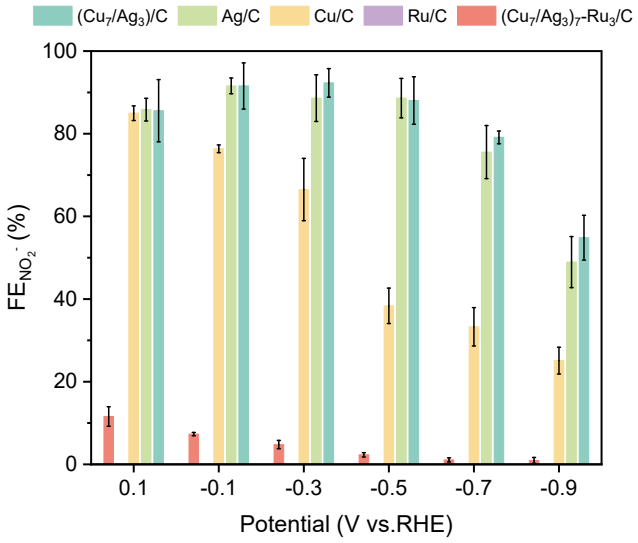

Figure S9. NO_2^- FEs for $(Cu_7/Ag_3)/C$, Cu/C, Ag/C, Ru/C, $(Cu_7/Ag_3)_7$-Ru_3/C at different applied potentials.

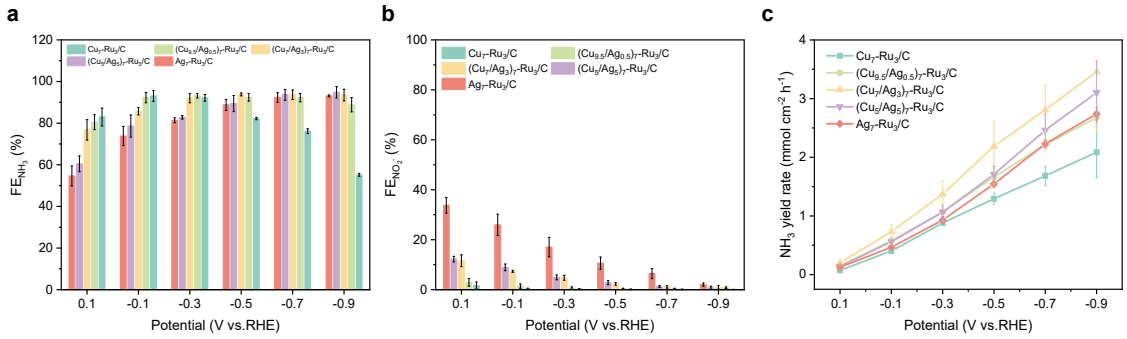

Figure S10. FEs of (a) NH_3, (b) NO_2^- and (c) the yield rates of NH_3 for Cu_7-Ru_3/C, $(Cu_{9.5}/Ag_{0.5})_7$-Ru_3/C, $(Cu_7/Ag_3)_7$-Ru_3/C, $(Cu_5/Ag_5)_7$-Ru_3/C and Ag_7-Ru_3/C at different applied potentials.

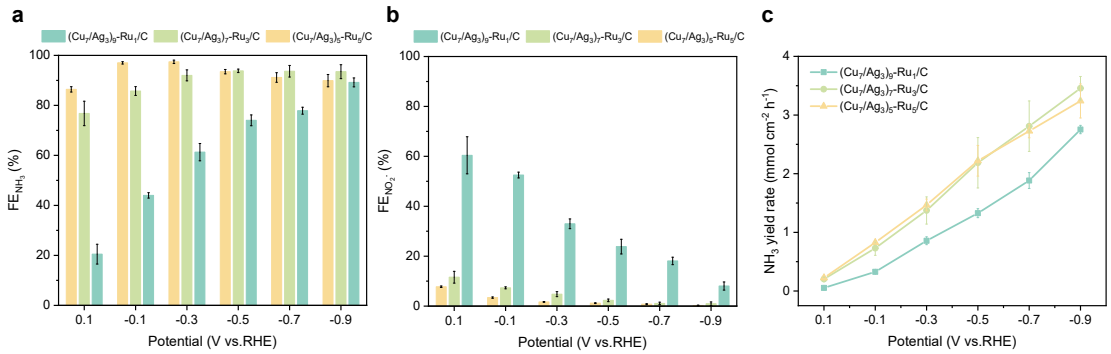

Figure S11. FEs of (a) NH_3, (b) NO_2^- and (c) the yield rates of NH_3 for $(Cu_7/Ag_3)_9$-Ru_1/C, $(Cu_7/Ag_3)_7$-Ru_3/C and $(Cu_7/Ag_3)_5$-Ru_5/C at different applied potentials.

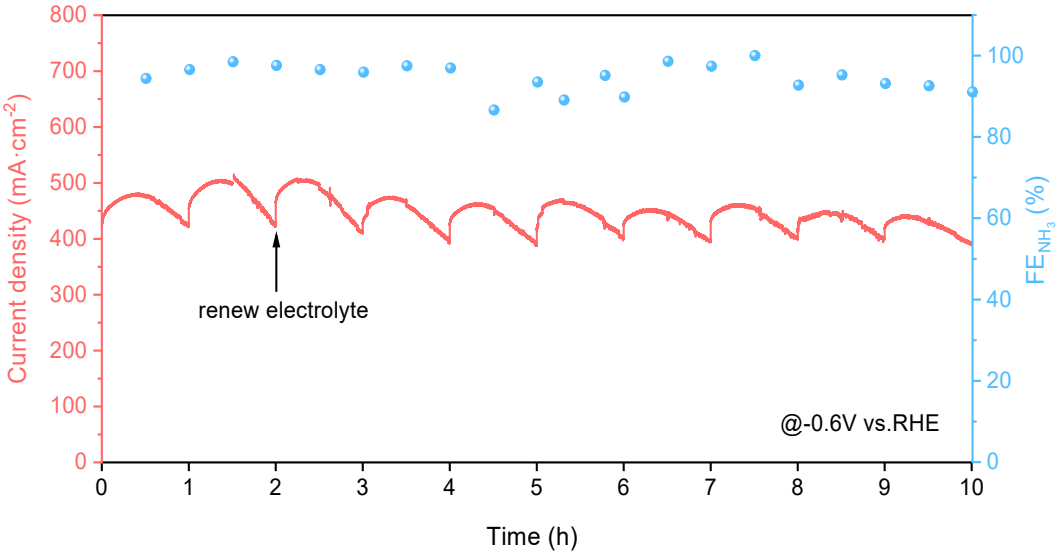

Figure S12. Short-term cycling stability testing of $(Cu_7/Ag_3)_7$-Ru_3/C.

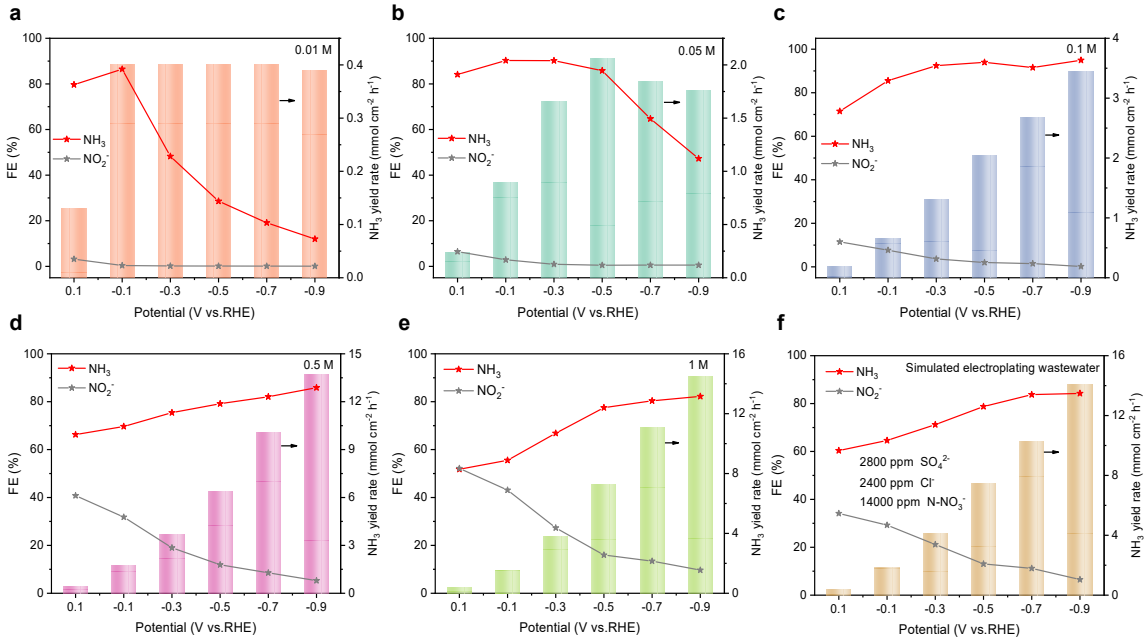

Figure S13. (a-e) FEs of NH_3 and NO_2^- as well as NH_3 yield rates in different concentration of NO_3^- with 1 M KOH under various potentials. (f) FEs of NH_3 and NO_2^- as well as NH_3 yield rates in simulated electroplating wastewater under various potentials.

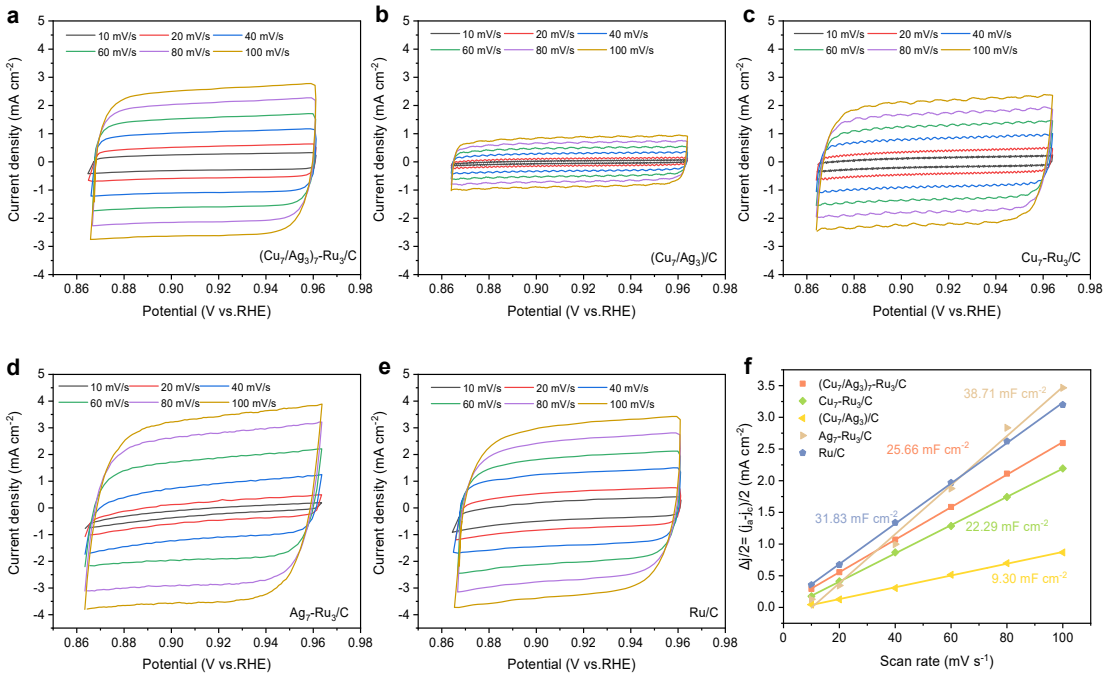

Figure S14. (a-e) Cyclic voltammetry curves of five catalysts at different scan rates. (f) Current density differences at 0.91 V vs. RHE against scan rates to calculate C_{dl}.

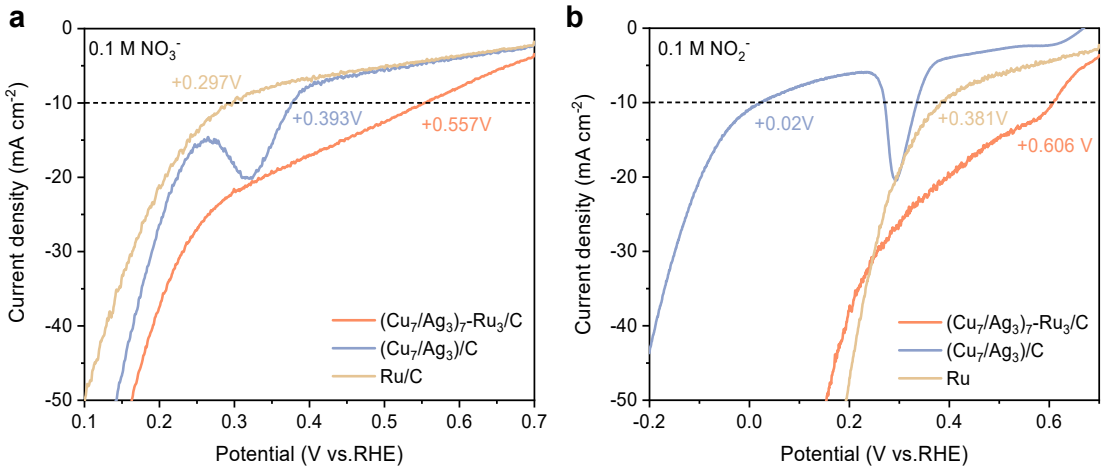

Figure S15. LSV curves at low current density in (a) 0.1 M NO_3^- and (b) 0.1 M NO_2^-.

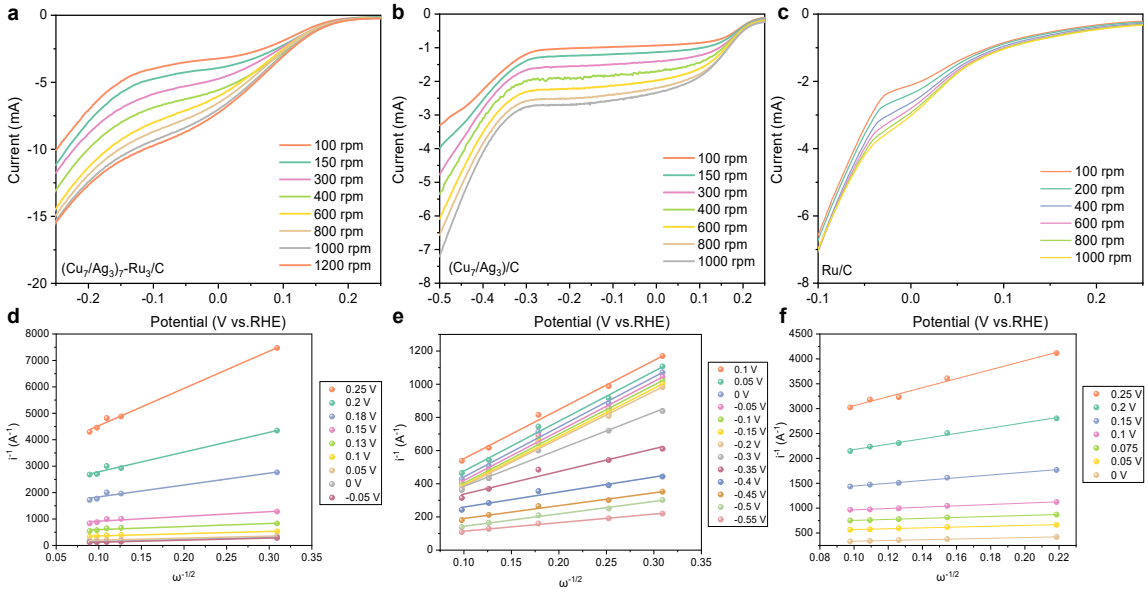

Figure S16. (a-c) LSV curves under different rotation rates of $(Cu_7/Ag_3)_7$-Ru_3/C, (Cu_7/Ag_3)/C, and Ru/C. (d-f) The data fitting of electron transfer number estimation.

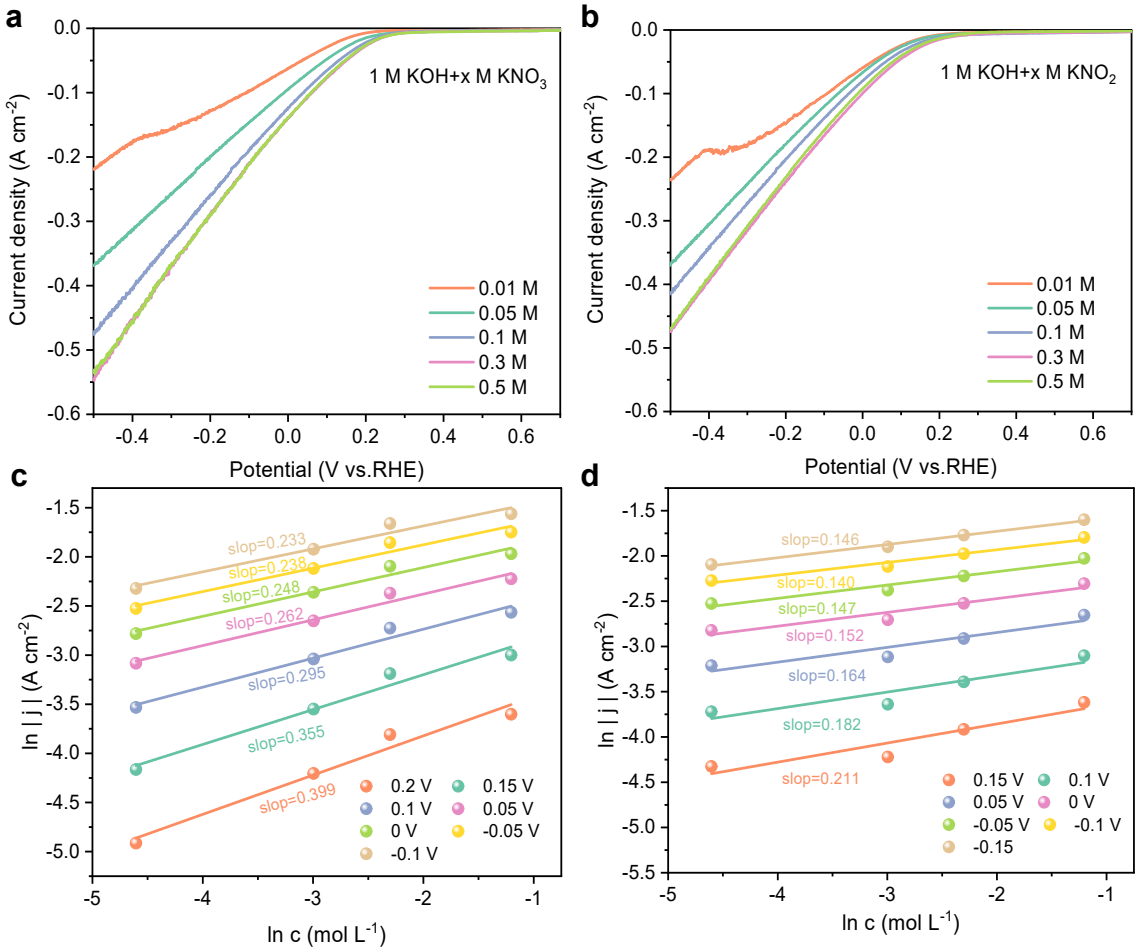

Figure S17. (a,b) LSV curves of $(Cu_7/Ag_3)_7$-Ru_3/C in different concentrations of nitrate or nitrite under a stirring of 800 rpm. (c,d) Linear fit of ln[j] against ln[c] to obtain the reaction rate order.

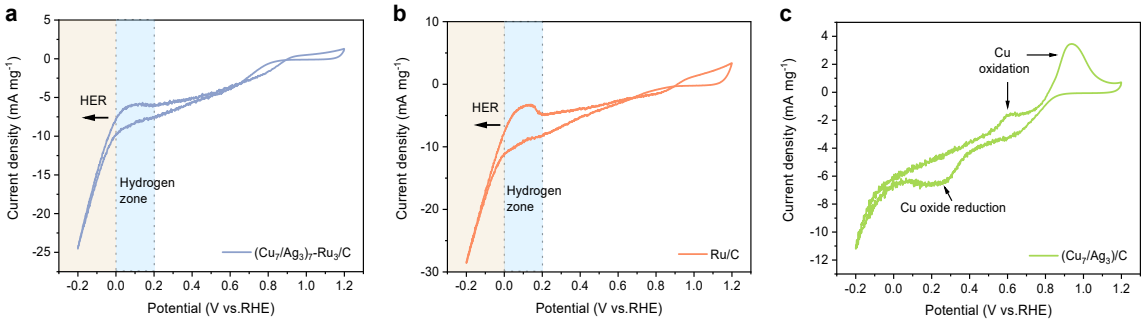

Figure S18. CV curves of (a) $(Cu_7/Ag_3)_7$-Ru_3/C, (b) Ru/C and (c) (Cu_7/Ag_3)/C in 0.1 M KOH solution with a 5 mV s^{-1} sweeping speed.

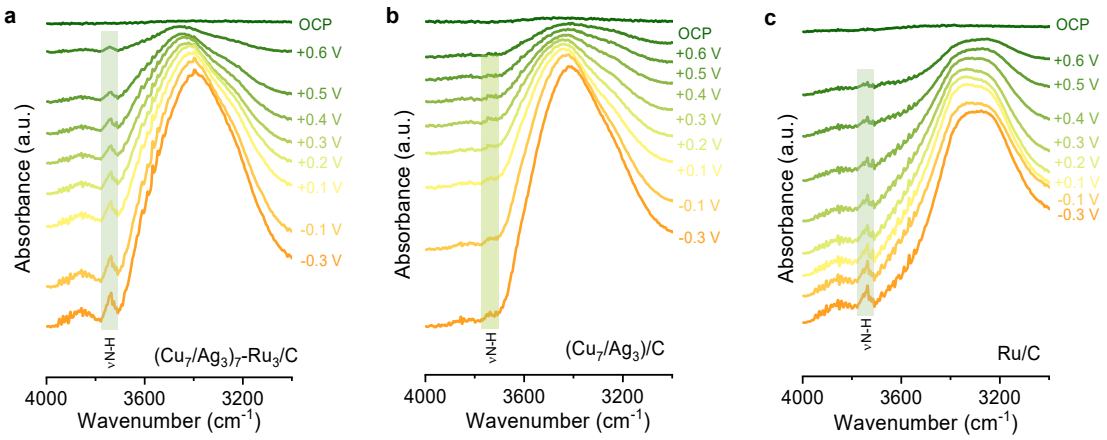

Figure S19. Infrared signals in the range of 3000-4000 cm^{-1} over (a) $(Cu_7/Ag_3)_7$-Ru_3/C, (b) Ru/C, and (c) (Cu_7/Ag_3)/C in 1 M KOH + 0.1 M KNO_3.

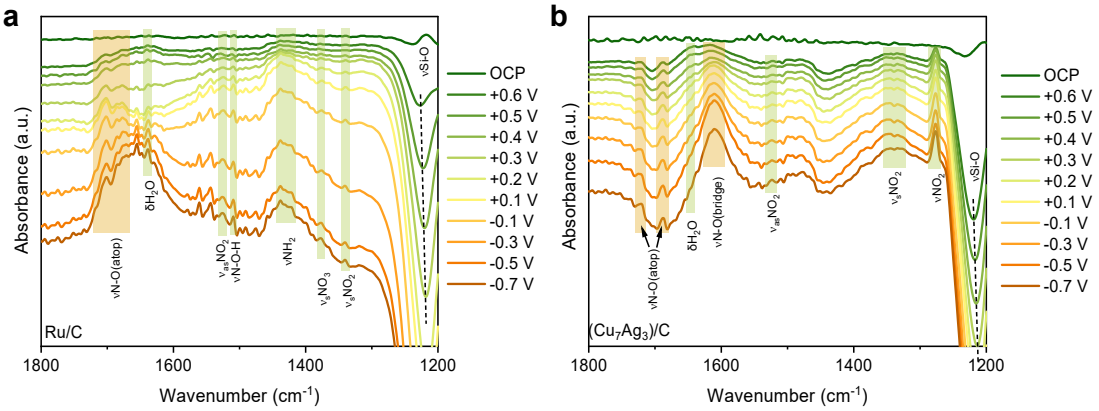

Figure S20. Infrared signals in the range of 1800 to 1200 cm^{-1} over (a) Ru/C and (b) $(Cu_7/Ag_3)/C$, in 1 M KOH + 0.1 M KNO_2.

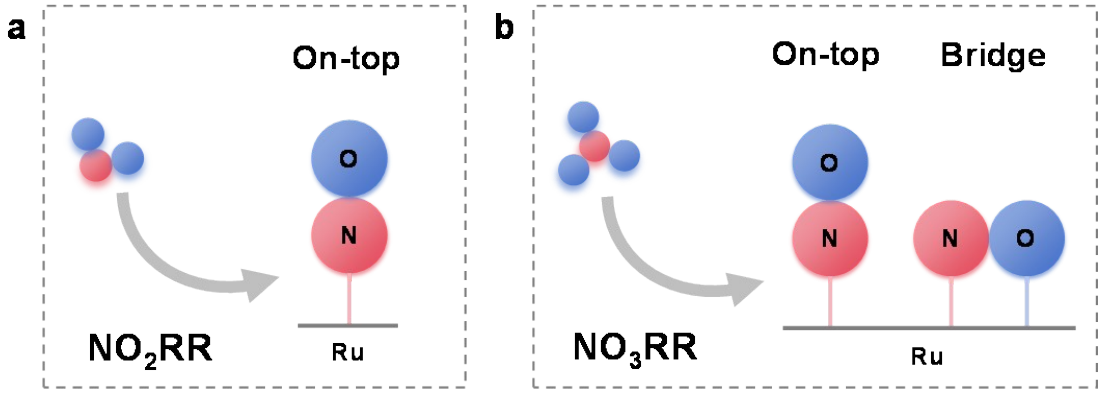

Figure S21. The different configuration of NO formed on the surface of Ru in (a) NO_2RR and (b) NO_3RR.

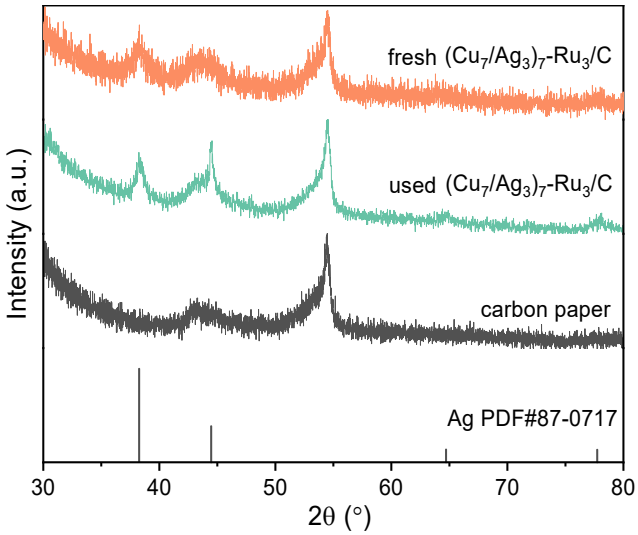

Figure S22. XRD patterns of $(Cu_7/Ag_3)_7$-Ru_3/C before and after 60-hour stability test and carbon paper.

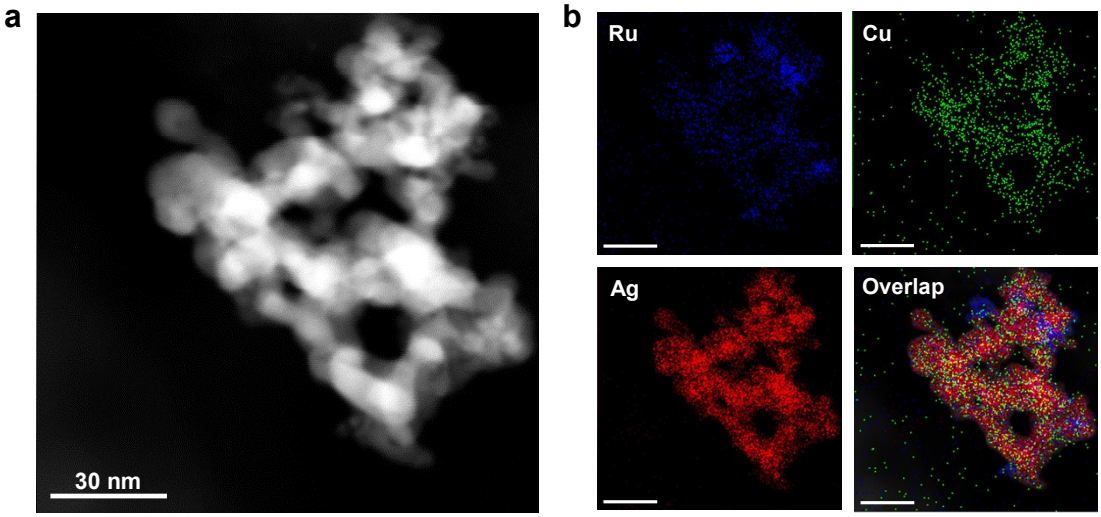

Figure S23. (a) The TEM and (b) EDX mapping images of $(Cu_7/Ag_3)_7$-Ru_3/C after 60-hour stability test.

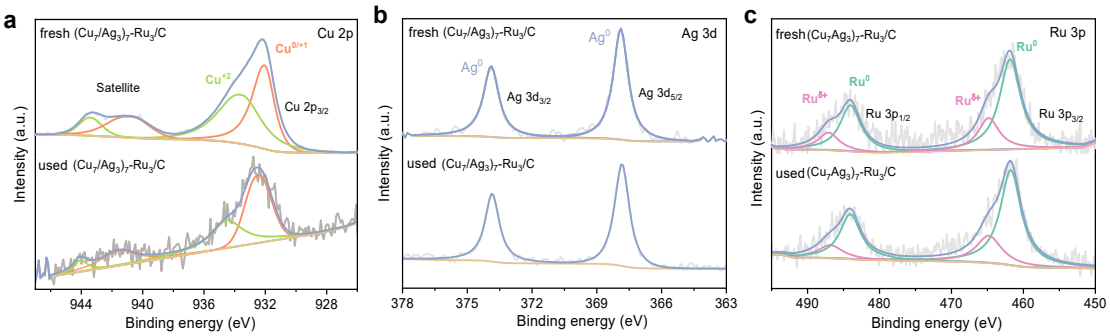

Figure S24. The XPS spectra of (a) Cu 2p, (b) Ag 3d, and (c) Ru 3p before and after 60-hour stability test.

Table S1. The NO_3RR performance comparisons between the $(Cu_7/Ag_3)_7$-Ru_3/C with other reported catalysts.

Catalyst	Electrolyte	FE (%)	NH_3 yield rate ($mmol \cdot h^{-1}\ cm^{-2}$)	NH_3 yield rate ($mol \cdot h^{-1}\ g_{cat}^{-1}$)	Ref.
$(Cu_7/Ag_3)_7$-Ru_3/C	1 M KOH + 0.1 M KNO_3	92.42 @-0.3 V	1.31	0.873	This work
$(Cu_7/Ag_3)_7$-Ru_3/C	1 M KOH + 0.1 M KNO_3	94.93 @-0.9 V	3.45	2.30	This work
Ru/Cu_2O	1 M KOH + 1 M KNO_3	~100 @-0.2 V	2.18	-	7
Cu/Cu_2O NWAs	1 M KOH + 200 ppm NO_3^-	95.8 @-0.85 V	0.2449	-	8
Ru_1Cu_{10}/rGO	1 M KOH + 0.1 M KNO_3	98 @-0.05 V	0.38	0.38	9
Cu-NBs-100	1 M KOH + 0.1 M KNO_3	95 @-0.15 V	1.3	0.655	10
Strained Ru nanoclusters	1 M KOH + 1 M KNO_3	45 @-0.8 V	1.17	5.56	11
Rh/Cu nanowires	0.1 M Na_2SO_4+ 0.1 M NO_3^-	70 @-0.4 V	1.27	-	12
$NiMoO_4/CuO$ NW/CF	1 M KOH + 0.05 M KNO_3	98.8 @-0.2 V	0.8221	-	13
$Ru_{15}Co_{85}$ HNDs	1 M KOH + 0.1 M KNO_3	97 @0 V	1.926	3.21	14
$Ag/Co_3O_4/CoOOH$ NWs	1 M KOH + 0.1 M KNO_3	94.3 @-0.25 V	0.2537	-	15
Ag_9 NCs	0.5 M K_2SO_4+ 50 ppm N-NO_3^-	80.2 @-0.95 V	-	-	16
AuCu@Ag NWs	1 M KOH + 50 ppm N-NO_3^-	96.9 @-0.2 V	-	0.057	17
Cu/Cu_2O	0.1 M PB + 0.1 M KNO_3	93.9 @-0.9 V	0.2198	-	18

References

1. L. Li, C. Tang, X. Cui, Y. Zheng, X. Wang, H. Xu, S. Zhang, T. Shao, K. Davey and S.-Z. Qiao, *Angew. Chem. Int. Ed.*, 2021, **60**, 14131-14137.
2. O. Q. Carvalho, R. Marks, H. K. K. Nguyen, M. E. Vitale-Sullivan, S. C. Martinez, L. Árnadóttir and K. A. Stoerzinger, *J. Am. Chem. Soc.*, 2022, **144**, 14809-14818.
3. S.-E. Bae, K. L. Stewart and A. A. Gewirth, *J. Am. Chem. Soc.*, 2007, **129**, 10171-10180.
4. D. Pletcher and Z. Poorabedi, *Electrochim. Acta*, 1979, **24**, 1253-1256.
5. Y. Wang, A. Xu, Z. Wang, L. Huang, J. Li, F. Li, J. Wicks, M. Luo, D.-H. Nam, C.-S. Tan, Y. Ding, J. Wu, Y. Lum, C.-T. Dinh, D. Sinton, G. Zheng and E. H. Sargent, *J. Am. Chem. Soc.*, 2020, **142**, 5702-5708.
6. M. Chatenet, M. B. Molina-Concha, N. El-Kissi, G. Parrour and J. P. Diard, *Electrochim. Acta*, 2009, **54**, 4426-4435.
7. Q. Hu, K. Yang, O. Peng, M. Li, L. Ma, S. Huang, Y. Du, Z.-X. Xu, Q. Wang, Z. Chen, M. Yang and K. P. Loh, *J. Am. Chem. Soc.*, 2023, **146**, 668-676.
8. Y. Wang, W. Zhou, R. Jia, Y. Yu and B. Zhang, *Angew. Chem. Int. Ed.*, 2020, **59**, 5350-5354.
9. W. Gao, K. Xie, J. Xie, X. Wang, H. Zhang, S. Chen, H. Wang, Z. Li and C. Li, *Adv. Mater.*, 2023, **35**, 2202952.
10. Q. Hu, Y. Qin, X. Wang, Z. Wang, X. Huang, H. Zheng, K. Gao, H. Yang, P. Zhang, M. Shao and C. He, *Energy Environ. Sci.*, 2021, **14**, 4989-4997.

11. J. Li, G. Zhan, J. Yang, F. Quan, C. Mao, Y. Liu, B. Wang, F. Lei, L. Li, A. W. M. Chan, L. Xu, Y. Shi, Y. Du, W. Hao, P. K. Wong, J. Wang, S.-X. Dou, L. Zhang and J. C. Yu, *J. Am. Chem. Soc.*, 2020, **142**, 7036-7046.
12. H. Liu, X. Lang, C. Zhu, J. Timoshenko, M. Rüscher, L. Bai, N. Guijarro, H. Yin, Y. Peng, J. Li, Z. Liu, W. Wang, B. R. Cuenya and J. Luo, *Angew. Chem. Int. Ed.*, 2022, **61**, e202202556.
13. C. Lin, X. Chen, L. Wang, W. Li, Z. Wang, M. Li, J. Feng, B. Hou and W. Yan, *Adv. Funct. Mater.*, 2024, **34**, 2401287.
14. S. Han, H. Li, T. Li, F. Chen, R. Yang, Y. Yu and B. Zhang, *Nat. Catal.*, 2023, **6**, 402-414.
15. S. Wu, Y. Jiang, W. Luo, P. Xu, L. Huang, Y. Du, H. Wang, X. Zhou, Y. Ge, J. Qian, H. Nie and Z. Yang, *Adv. Sci.*, 2023, **10**, 2303789.
16. L. Liu, S.-J. Zheng, H. Chen, J. Cai and S.-Q. Zang, *Angew. Chem. Int. Ed.*, 2024, **63**, e202316910.
17. S. Liu, W. Miao, K. Ma, H. Teng, X. Zhang, J. Li, W. Li, X. Cui and L. Jiang, *Appl. Catal. B Environ.*, 2024, **350**, 123919.
18. N. Zhou, Z. Wang, N. Zhang, D. Bao, H. Zhong and X. Zhang, *ACS Catal.*, 2023, **13**, 7529-7537.